Reply to D. Rosenfeld

We thank D. Rosenfeld for reading our manuscript and for his helpful comments and suggestions. Please find below a discussion of the reviewer's comments (italic lines). Changes/additions made to the text are underlined.

1. It is shown that the ice index in the simulations is decreased and the sensitivity to effective radius fades away for small water or ice water content. Please explain the causes for that.

We have rewritten the discussion about the profile of the phase index (formerly called ice index) for the inhomogeneous cloud case as follows:

<u>The differences of the phase index for the ice layer depend strongly on the effective radius. Large effective radii (as at the bottom of the layer) result in a strong absorption due the decrease of the single scattering albedo. Also the mixed-phase layer can be identified. The variation of the phase index with height for the region of liquid phase is low (-0.13 to -0.01) compared to the mixed-phase zone, where the phase index changes rapidly from negative to positive values (-0.01 to 0.31). When reaching the region with pure ice-phase, the change of Ip with height is again reduced compared to the mixed-phase layer. However, in the most upper part of the cloud with ice particles of reff < 20 µm the phase index could be misinterpreted as liquid particles. Here, the single scattering albedo (ω = 0.98) of the small ice particles approaches values that are in the lower range of large liquid particles. In addition to the variable LWC/IWC (open circles in Fig. 6c) also simulations with fixed water content (0.7 g m−3) are performed. Their difference is largest in the mixed-phase layer and at the top of the cloud where the variable IWC is much lower than 0.7 g m−3. Low extinction due to low IWC at cloud top causes a decrease of the phase index compared to the simulation with fixed water content. A steady decrease of IWC tends to result in a phase index that is similar to a phase index which would be derived for clear sky conditions. There, the phase index depends mainly on the slope of the downward solar spectrum between 1550 and 1700 nm. This negative slope leads to a negative ice index pretending the liquid cloud phase. In the mixed-phase layer of the cloud the impact of the water content gets obvious. Depending on the amount of LWC and IWC either the spectral extinction of the liquid or the ice particles are dominating the phase index. In the lower part of the mixed-phase layer (with LWC >> IWC) the phase index is shifted to lower values compared to the simulations with a constant water content, while in the upper part of mixed-phase layer the phase index is shifted to higher values.</u>

2. A major point of this study is the validation of the inferred phase by the retrieved ice index by the lidar depolarization ratio, delta. However, only three hand picked selected points are given in Table 2. The study will be much more informative if additional figure similar to Figure 7 will be added, but where time intervals during which the observations were made out of cloud or in shadowed clouds will be masked, and the time series of the delta parameter will be added. Without this, the demonstration of the validity of the method remains rather weak.

With respect to the former Fig. 7, we prefer not to show the time-series of the lidar depolarization slope in this context because during this specific measurement case the situation was too complex (inhomogeneous both spatial and temporal) to derive a consistent picture from these data. Just to give some numbers: The time resolution of the spectrometer measurements was below two seconds, while one lidar profile was sampled within 30 seconds. Mostly, individual clouds did not last longer than two minutes. A convolution of the spectrometer data in terms of the temporal resolution of the lidar did not point out the small scale variation of the phase index in most of the cases. Therefore we restricted the comparison between phase index and lidar depolarization slope to these three cases.

However, we added a discussion about the identification of the shadows for this specific measurement case (Fig.7) and color-coded the phase index in Fig. 8, to indicate the different observing situations (illuminated, shadow, cloud-free).

The data interpretation is supported by photos which also help to sort out shadowed cloud portions which cannot be used for phase discrimination due to the contamination of the spectral slopes of the radiances which are used for the phase discrimination. For fully illuminated, non-shadowed cloud elements the spectral signature of the reflected signal depends mainly on the spectral signature of the downward solar radiation and its spectral extinction by the observed cloud element. In contrast, for shadowed cloud elements the incident radiation is mostly determined by diffuse radiation. This diffuse radiation is strongly affected by the spectral extinction of the shadowing cloud element but may also be affected by the spectral surface albedo. To identify the illuminated cloud portions all measured spectra were classified with respect to possible contaminations. Fig. 7a shows examples of measured spectra for different targets: fully illuminated cloud side, shadowed cloud parts, overcast situation, and no cloud. In particular the absolute value of the radiances in the visible spectral range and the slope of the spectrum between 500 and 880 nm reveals significant differences between the four spectra. In this spectral range the radiance reflected from the illuminated cloud part decreases with increasing wavelength whereas for spectra with contamination by other clouds the radiance shows an increase at about 730 nm. This feature is an effect of the interaction between clouds and a surface albedo which is affected by vegetation in this particular case. Spectra observed under cloudless conditions show the typical nonlinear decay of the radiance in the VIS caused by Rayleigh scattering. To quantify the spectral differences between reflected radiation from shadowed and illuminated cloud parts, all spectra were normalized to the radiance at 480 nm. Fig. 7b shows the ratio between the normalized spectra and a normalized spectrum of an illuminated cloud scene. As expected, the most significant difference is observed for the cloudless observation. The overcast situation is characterized by a strong decrease of the ratio in the NIR (ratio < 0.5 above 1100 nm). To distinguish the cloud scenes the radiance ratios at two wavelengths (857 nm and 1550 nm, vertical dashed lines in Fig. 7) were calculated. For ratios between 0.8 and 1.2 the cloud scene was defined as illuminated, whereas cloudless situations were identified for ratios lower than 0.5. All other spectra were classified as shadowed/overcast cloud scenes.

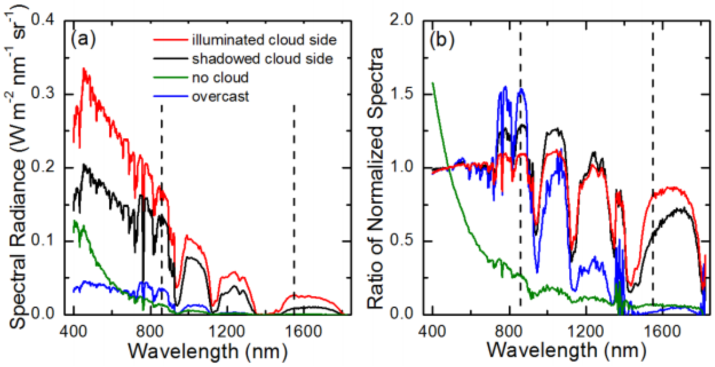

Fig. 7. (a) Spectra of different observing situations: illuminated cloud side, cloud shadow, overcast, and view out of cloud. (b) Normalized spectral ratios for the cloud scenes from (a) related to a spectrum of illuminated cloud side.

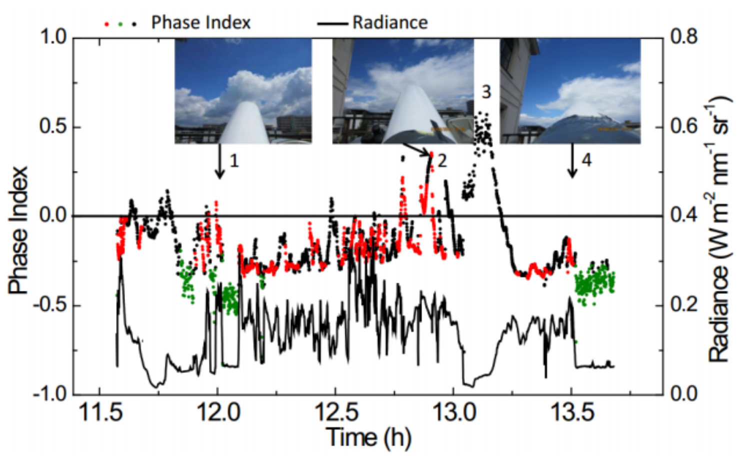

Fig. 8. Time series of spectral radiance at 550 nm wavelength (black line) and derived phase index (colored circles). The colors indicate the different observing situations: illuminated cloud side (red), cloud shadow/overcast (black), and cloud-free in viewing direction (green).